# On the in-plane tear test

HEIKKI KETTUNEN AND KAARLO NISKANEN

## ABSTRACT

*In the in-plane tear test, one forces a crack through a long ligament of paper. The tearing energy per unit of crack length varies with the tearing angle. We show that in brittle papers the tearing energy increases with roughness and branching in the fracture line. In tough papers, additional energy is expended as a result of plastic elongation, or "damage," outside the fracture process zone. If these aberrations are avoidable with a suitable tearing angle, the corresponding "true" or minimum tearing work characterizes a microscopic process in which the paper breaks completely. In the samples we studied, tearing energy was 20% larger than the critical fracture energy measured with the J-integral method. We claim that neither the macroscopic geometry nor the dynamics of the tear test can explain this difference. Its origin must lie in the microscopic fracture process that is different between the in-plane tear test and the J-integral method.*

***Application:***

*Exploring inconsistencies in tear test methods may lead to better means for measuring strength properties.*

THE TEAR TEST MEASURES THE energy dissipated when a crack is forced to propagate through a paper specimen. The theory of forced crack propagation suggests that the tearing work should be larger than, or at least equal to, the critical fracture energy of paper. The critical fracture energy is often called the "fracture toughness" of paper (*1*) and is the amount of energy necessary to overcome the paper's resistance to tearing. As a measure of fracture toughness, the simple in-plane tear test is attractive because its relationship to crack propagation is easy to comprehend. However, the test may overestimate tearing work.

One of the first studies on the in-plane tear test was published by Unger in 1960 (*2*). In 1967, Van den Akker and colleagues published a paper that made the method commonly known (*3*). Experimentally, the in-plane tearing work depends on the test geometry. Van den Akker and coworkers tested machine-made papers at tearing angles from 3° to 19°. They concluded that a 12° tearing angle in combination with a 50-mm span length is best for most paper grades. The short span length minimized the energy dissipation outside the fracture process zone, and the 12° angle corresponded to a broad minimum in the tearing work. In the wake of Van den Akker's work, the 12° tearing angle has become a *de facto* standard in the tear test. Since then, other experiments have been reported (*1, 4–7*).

In our study, we wanted to find out why the in-plane tearing work varies with tearing angle. Is there a tearing geometry for which the tearing work measured is equal to the critical fracture energy as measured by some other method? If the equality cannot be achieved by the proper choice of test geometry, then the difference between the two should provide useful information about microscopic fracture processes. Such information is particularly interesting because the tear test allows stable crack propagation and gives long crack paths for microscopic analysis (*8*).

These factors motivated our study of the in-plane tear test. However, we do not advocate the tear test as the most valid test for measuring the fracture toughness.

## BACKGROUND ON THE TEAR TEST

**Figure 1** shows the principle of the in-plane tear measurement. The specimen is clamped so that the jaws form an angle of $2\alpha$ before the shorter edge of the specimen is pulled tight. The longer edge is slack, and it bends out of the test plane by an amount that depends on the tearing angle and the dimensions of the specimen.

When the external displacement increases, the paper breaks first at the notch tip. After this initial phase in which the force increases, the crack grows through the specimen (from left to right in Fig. 1) as the displacement increases. During this second phase, the external load is carried by a narrow section, or "neck," between the crack tip and the slack area. The overall crack propagation is stable. External displacement controls the position of the crack tip. This phase continues until the slack end of the specimen begins to get tight. Finally, in the third phase, the force decreases to zero as the load-carrying neck gradually narrows and vanishes.

**Figure 2** shows the curves for measured force vs. displacement for total tearing angles of 2°, 5°, and 15°. These examples reflect the three phases of the tearing process. The ligament was 80 mm long, and tearing was in the machine direction.

Kärenlampi *et al.* gave a simple trapezoidal model for the force–displacement behavior (*1*). In his dissertation, Kärenlampi analyzed the

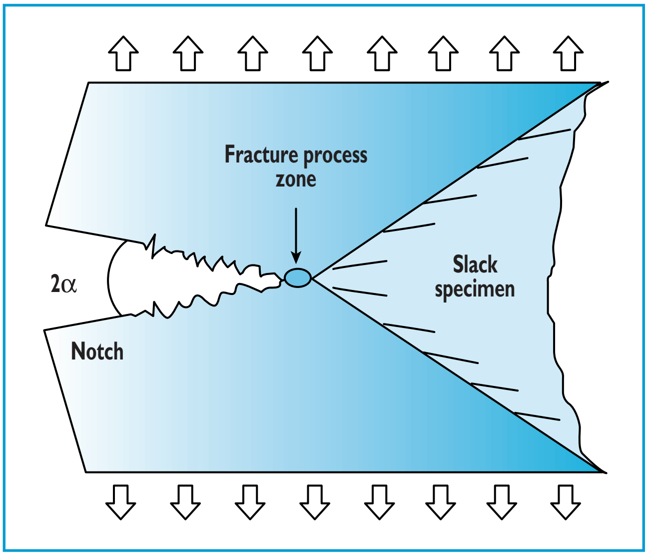


*1. Geometry of the in-plane tear measurement.*

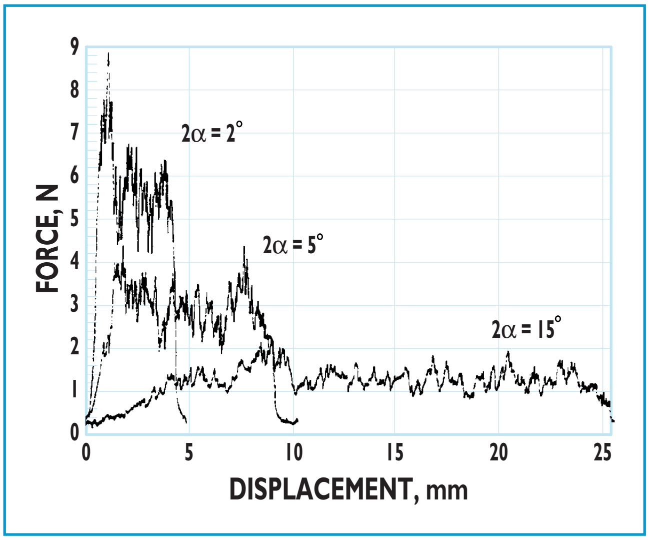


*2. Force–displacement curves of magazine paper at tearing angles of 2°, 5°, and 15°.*

behavior in more detail using a numerical linear elastic model (*9*). In the appendix, we give a detailed analytical solution. All of the models suggest that during stable crack propagation the tearing force $F$ is inversely proportional to tan $\alpha$, where $\alpha$ is the tearing angle (of a single side, from the horizontal).

The area under the force–displacement curve is the tearing work $W$. Work $W$ divided by the ligament length $L$ gives the tearing work per unit crack length, $dW/dL$. Equation 1 describes the relationship between $dW/dL$ and tearing force and tearing angle:

$$dW/dL = 2F \tan\alpha \qquad (1)$$

Thus the tearing work per unit crack length should be independent of the tearing angle $\alpha$. In fact, our model analysis suggests that the fracture process zone is microscopic for practically all total tearing angles of $2\alpha \geq 2°$. Therefore, the macroscopic test geometry should not affect the fracture process zone or the energy dissipated in the zone. In contradiction to the theoretical predictions however, the tearing angle usually has a clear effect on the measured tearing work. One task, then, is to explain the reasons for the dependence on the size of the angle, which is inconsistent with the model predictions.

There are two ways to measure and derive the tearing work per unit crack length. One can measure the average tearing force, excluding the initial and final phases, and multiply the result by 2 tan $\alpha$. Alternatively, one can also use different tearing angles and then determine the slope of $dF/d(2 \tan\alpha)^{-1}$, which is equal to $dW/dL$. The two methods give the same result, provided that geometric effects are absent. One can choose any angle and obtain the same result as that from tests in which various angles are used.

## EXPERIMENTAL PROCEDURES

### Mechanical testing

We used an ordinary tensile testing machine (L&W TCT-5) equipped with linear guides to prevent the specimen from twisting, shearing, and rotating in the in-plane test. For most of the measurements, the span length at the shorter edge of the specimen was 45 mm, and the specimen width was 105 mm. The width included a 25-mm initial cut in the middle of the shorter edge, so the ligament length (and thus the crack length) was 80 mm. The displacement rate was 10 mm/min.

Tearing angles ranged from 0° to 20°, with accuracy of ±0.5°. Tearing angles larger than 20° were not possible because they led to large force fluctuations and thus to erratic crack growth, especially with stiff paper grades. We also varied the ligament length over a range from 20 mm to 80 mm in a separate set of tests.

We measured five parallel specimens in each case. Particularly at small angles ($2\alpha \leq 2°$), force fluctuations made it difficult to determine the range over which the average force should be calculated. Some variability in the force values at small tearing angles also arises from the uncertainty in setting the value of $\alpha$. The ranges for the standard deviations of the average tearing forces reported are 10–20% for $2\alpha \leq 5°$ and 5–10% for large angles.

We followed SCAN-P 67:93 for tensile strength measurements and SCAN-P 77:95 for J-integral measurements. The standard laboratory conditions, 50% relative humidity and 23°C, prevailed in all the mechanical tests.

### Detection of damage

We impregnated samples with silicone to make visible the fracture process zone characterized by bond ruptures, which are termed "damage" here. In impregnation, the silicone (General Electrics RTV 615) fills almost all of the voids in paper. The paper becomes translucent as the silicone removes light-scattering surfaces. This change enhances the optical contrast of any free surface that may be created when the paper specimen is elongated. The same technique has been used in formation-scale studies (*10*, *11*), demonstrating how bond ruptures dominate the creation of new surface areas in impregnated paper.

We recorded the damage created in the tear tests with an ordinary desktop scanner. The images were scanned against a black background, and areas of damage are light gray or white. Undamaged areas are darker gray, with the density of the shade depending on paper grammage.

### *Sample material*

We used five machine-made papers, as listed in **Table I**, testing them in both the machine and cross-machine directions. Please notice that the columns are designated "MD" where the paper is loaded in the machine direction and the crack propagates in the cross-machine direction. Conversely, for the values in the "CD" columns, the paper is loaded in the cross direction, but the crack propagates in the machine direction.

| — | Grammage, | Breaking strain, % | | Elastic strain, % | |
|---|---|---|---|---|---|
| | g/m² | MD | CD | MD | CD |
| Magazine* | 65 | 0.96 | 1.9 | 0.65 | 0.69 |
| Newsprint | 45 | 0.92 | 2.1 | 0.69 | 0.95 |
| LWC | 65 | 1.1 | 2.1 | 0.64 | 0.62 |
| Pergament | 40 | 1.63 | 9.7 | 0.91 | 1.11 |
| Kraft | 70 | 2.3 | 5.4 | 1.01 | 1.06 |

*Supercalendered.

***I. List of the paper grades and the ordinary and elastic breaking strain***

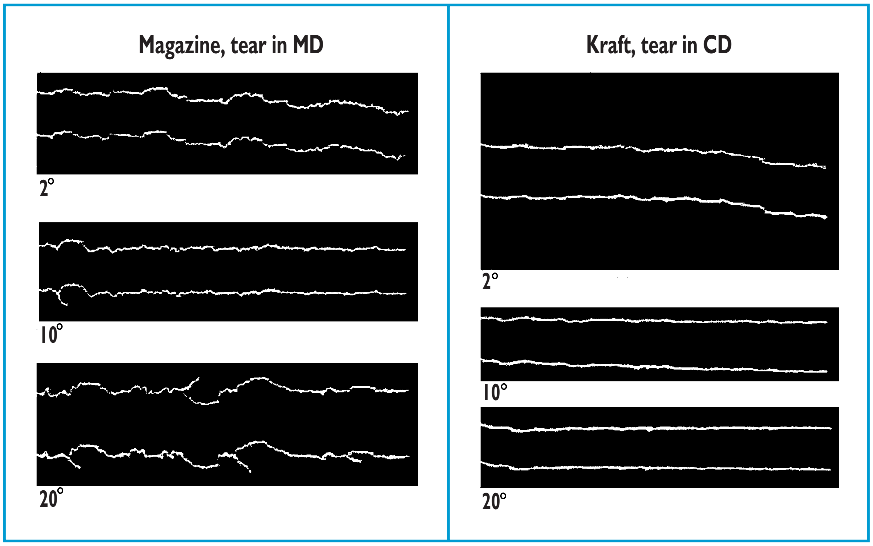


***3. Crack path, running from left to right, and damage in silicone-treated specimens: magazine paper in the machine direction (left) and kraft paper in the cross-machine direction (right). (Tearing angles of 2$\alpha$ = 2°, 10°, and 20° from top to bottom, respectively).***

To characterize the load–elongation behavior of the papers, we give the ordinary and "elastic" breaking strains in Table I. The elastic breaking strain is equal to the tensile strength divided by the elastic modulus. In linearly elastic papers, the two breaking strains are close to each other. In plastically yielding papers, however, the elastic breaking strain is clearly smaller than the ordinary breaking strain. The first behavior is typical in the machine direction, and the latter is typical in the cross-machine direction.

## EXPERIMENTAL RESULTS

### *Crack path and damage*

**Figure 3** illustrates damage created in crack propagation through a particularly brittle specimen, which is a magazine paper that was loaded in the machine direction, and a particularly tough specimen, a kraft paper loaded in the cross-machine direction. Here, toughness is judged from the ordinary and elastic breaking strain values in Table I.

The other papers listed in Table I showed patterns similar to the behavior exhibited in these two cases, one brittle and one ductile, or strong against the action of being pulled. Brittle specimens were the lightweight coated (LWC) and pergament in the machine direction and the newsprint and magazine paper in both directions. Ductile specimens were the kraft in the machine and cross-machine directions and the LWC and pergament in the cross direction.

The brittle magazine paper has a rough fracture line and somewhat unstable, intermittent crack propagation at small tearing angles. At $2\alpha \approx 10°$, the fracture line is smoother, and crack propagation is more stable. At still larger angles, the fracture line is rough again, and it has side branches. The branches extend 1–3 mm off the main crack. The branches are probably caused by the "blunt" shape of the in-plane stress field and possibly by constraints imposed by the out-of-plane buckling of the specimen. Out-of-plane buckling may also contribute directly to the measured energy consumption.

Crack propagation in the ductile kraft paper is different. The fracture line is smooth at all tearing angles and has no branches. When the tear-

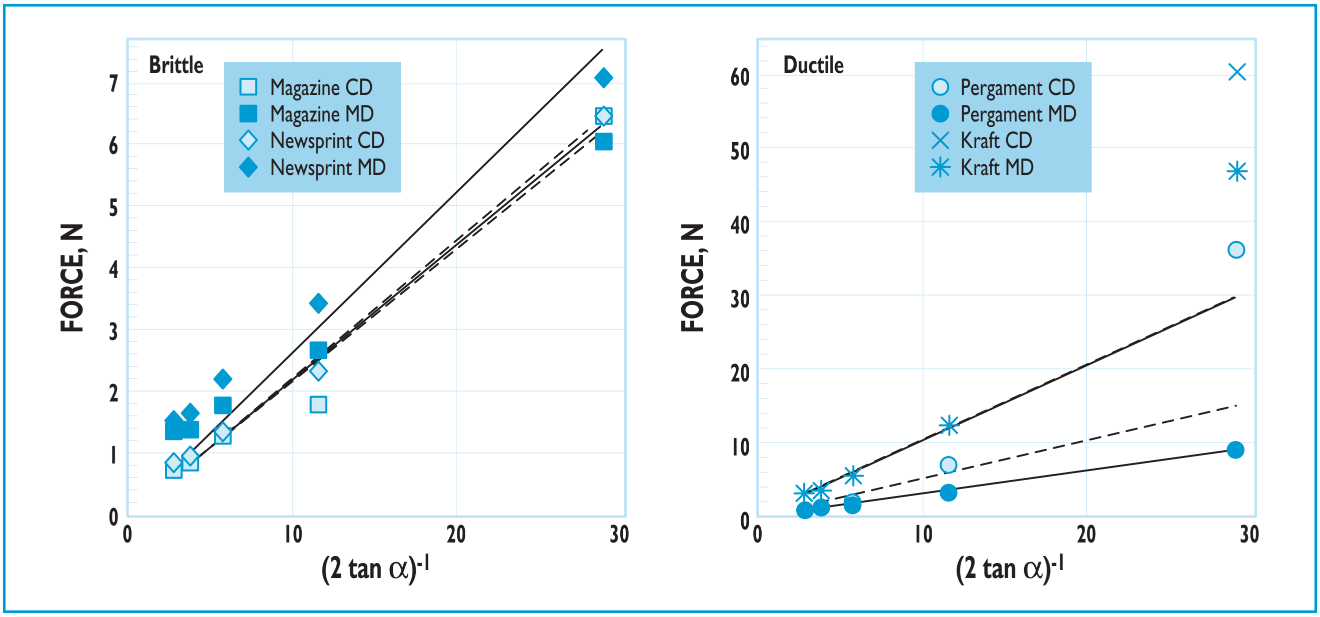


*4. Average tearing force against the inverse tangent of tearing angle $(2 \tan \alpha)^{-1}$, for the magazine paper, newsprint, pergament, and kraft paper. The lines show linear least-squares fits for each case, forced through the origin.*

ing angle is small, damage extends far from the fracture line, as can be seen in Fig. 3. Irreversible, plastic elongation has taken place in the damage areas, with related energy dissipation. Test geometry determines the shape of the damage area in kraft paper at small tearing angles. At large tearing angles, no damage occurs outside the fracture line.

In both papers, the width of the actual fracture line, seen as bright white in Fig. 3, is largely independent of tearing angle. It does not decrease with increasing $\alpha$ as macroscopic models predict. In our discussion in the appendix, we present the argument that the microscopic network structure should determine the fracture line width at $2\alpha \geq 2°$. This prediction is consistent with the examples in Fig. 3.

In summary, the effect that tearing angle has on tearing work for brittle papers probably arises from the shape of the fracture line. Roughness and branching both increase the "true" microscopic length of the fracture line. In tough papers, energy is consumed in damage outside the fracture line but only when the tearing angle is small. The fracture line itself is smooth at all tearing angles and should not cause any variation in tearing work.

| | Tearing work by the integral method, J/m | | Tearing work by the slope method, J/m | | J-integral fracture energy, J/m | |
|---|---|---|---|---|---|---|
| | MD | CD | MD | CD | MD | CD |
| Magazine | 0.29 | 0.21 | 0.22 | 0.22 | 0.18 | 0.15 |
| Newsprint | 0.40 | 0.26 | 0.27 | 0.23 | 0.27 | 0.16 |
| LWC | 0.39 | 0.36 | 0.35 | 0.34 | 0.26 | 0.31 |
| Pergament | 0.30 | 0.32 | 0.32 | 0.53 | 0.20 | 1.41 |
| Kraft | 1.07 | 1.07 | 1.05 | 1.06 | 1.22 | 1.06 |

*II. Values for tearing work per unit crack length and for J-integral fracture energy in the machine and cross-machine directions for all papers*

### *Tearing work*

**Figure 4** shows examples of the average tearing force $F$ against $(2 \tan \alpha)^{-1}$. Remember that models predict a linear relationship that goes through the origin. Many of the experimental results are consistent with this prediction. However, the brittle papers (magazine and newsprint in the machine direction) deviate from the linear trend close to the origin, when $(2 \tan \alpha)^{-1} < 6$, or when $2\alpha \geq 10°$. The ductile specimens (pergament in the cross direction and kraft paper in both directions) in turn deviate from the trend at small angles, $2\alpha \leq 4°$, or $(2 \tan \alpha)^{-1} > 15$. In both cases, the measured tearing force is larger than expected.

These deviations probably arise from crack branching in brittle specimens and from plastic damage in ductile specimens. In the first case, the crack tip propagates further than the specimen length would suggest. In the second case, the load-carrying neck is wider than it is for elastic papers.

The straight lines in Fig. 4 show the evaluation of tearing work per unit crack length using the slope of $F$ against $(2 \tan \alpha)^{-1}$. For ductile specimens, the point of largest $(2 \tan \alpha)^{-1}$

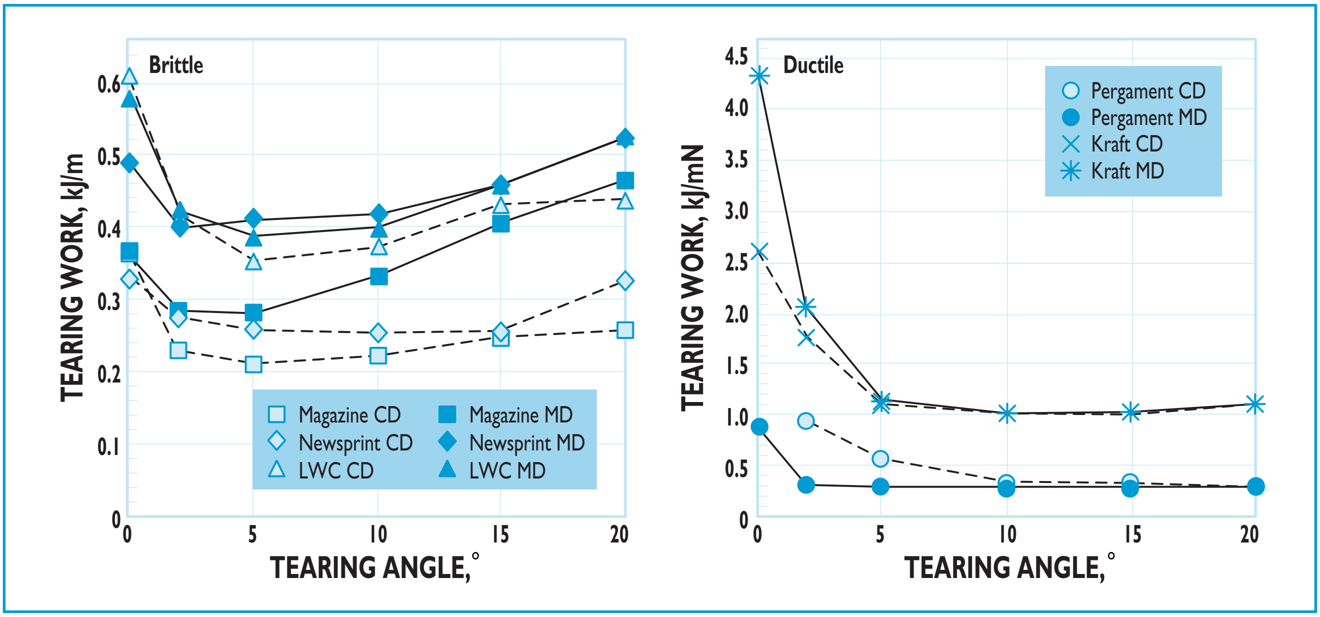


***5. Integrated tearing work per ligament length dW/dL against tearing angle 2α for magazine paper, newsprint, LWC, pergament, and kraft paper.***

(and smallest $\alpha$) is excluded from the fit. The result is, by construction, independent of $\alpha$, but as the figure shows, the accuracy is not good.

The corresponding results of the integral method are shown in **Fig. 5**. In this case, the tearing work per unit crack length is obtained from the area under the load-displacement curve divided by the ligament length *L*. In the brittle papers, the tearing work has at least a weak minimum at some value of $\alpha$. In the ductile papers, there is practically no minimum.

The variation of tearing work with $\alpha$ agrees with the conclusions drawn from Fig. 3 above. The roughness and branching of the fracture line and the plastic damage outside the fracture line are the probable causes for the variation. For each paper, the smallest value of tearing work is the best estimate.

The two values for tearing work, one from the slope of *F* as plotted against $(2 \tan \alpha)^{-1}$ and the other from the integral of the load-displacement curve, are compared in **Table II**. They are quite close to each other in most cases. This outcome is not a trivial result. One method uses a range of tearing angles, and the other uses only the angle that corresponds to the minimum tearing work. When differences exist, the integral method gives the higher value. The largest differences are for newsprint in the machine direction and for pergament in the cross direction. The poor fit in Fig. 4 is probably the cause for the differences.

Table II also gives the J-integral fracture energies. These energies are generally smaller, but otherwise they correlate well with the in-plane tear results. The same correlation that exists between tearing work and J-integral applies also to the values reported by Kärenlampi *et al.* (*1*), who studied handsheets made of different kraft pulps.

On average, all of these results give a J-integral that is 20% smaller than the tearing work per unit of crack length. Only the pergament in the cross direction and kraft paper in the machine direction have clearly larger values for J-integral than for tearing work. They both have large plastic elongation in the tensile test, as Table I shows. We believe that the stress-strain curve of these papers does not show agreement with the Ramberg-Osgood model used in the J-integral measurement.

***Effect of ligament length***

Measured fracture energies often depend on specimen dimensions. We tested the effect of ligament length in the in-plane tear test using the magazine paper loaded in the machine direction. **Figure 6** shows the results for three tearing angles. The behavior is qualitatively similar to that seen, for example, in the essential work of fracture method (EWF) (*12*).

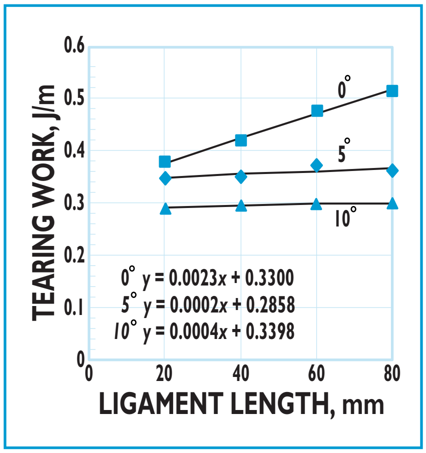


***6. Tearing work per unit of crack length against ligament length at tearing angles 2α = 0°, 5°, and 10° in the magazine paper loaded in the machine direction. (Linear regression equations are also shown.)***

From Fig. 6, we can infer that, at least in brittle papers, the measured tearing work depends on ligament length at small angles but not at large angles. Therefore the results in Figs. 4 and 5 at $2\alpha$ angles of 0° and 2° could have been different, had we considered a ligament length different from the 80 mm used. Interestingly, extrapolation to zero ligament length gives the same value for tearing work (to within ±10%) at the three tearing angles.

## DISCUSSION

One of our purposes was to explain why tearing angle affects the in-plane tearing work. We conclude that in brittle papers the effect arises from the shape of the fracture line. At $\alpha$ values that are too small or too large, the fracture line is rough. At large values of $\alpha$, side branches also appear. As a result, the true microscopic fracture path is longer than the ligament length of the specimen. In ductile papers, the fracture line is smooth at all $\alpha$, but instead plastic damage is created outside the fracture line if $\alpha$ is too small. All these factors lead to an overestimation of the critical fracture energy in the tear test. They should also contribute to the overestimation observed in tests conducted by the EWF method (*13*).

The integral under the load–displacement curve gives the physically most sensible value for the tearing work per unit crack length, provided that one can vary the tearing angle so as to obtain the minimum value of tearing work. In the samples we measured, this minimum value is, on the average, 20% higher than the critical fracture energy given by the J-integral method. Otherwise, the J-integral and in-plane tear values correlate quite well.

There are many factors that may explain the difference between J-integral and in-plane tear. For example, the macroscopic test geometry, particularly the out-of-plane deformations and nonzero tearing angle, may contribute even to the minimum value of in-plane tearing work. The credibility of this argument suffers from our finding, as explained in the appendix, that the fracture process zone is microscopic in size at all but the smallest tearing angles. Thus the macroscopic test geometry should not affect the microscopic fracture process in the case of minimum energy dissipation.

The experimental damage observations illustrated in Fig. 3 corroborate this prediction. The width of the actual fracture process zone (the bright zone next to the fracture line) does not appear to vary with the tearing angle. A more detailed analysis is under way to provide quantitative estimates of the size of the fracture process zone.

In principle, it is also possible that some of the elastic energy stored in the specimen converts directly to heat and does not promote crack propagation. This possibility would explain why tearing work per unit crack length is larger than the critical fracture energy. However, this mechanism should reveal itself as a sudden unstable acceleration of the crack at the end of the tear test. We observed no evidence of such an acceleration in the tear test nor in the crack paths in Fig. 3. Furthermore, our theoretical analysis explains why the load–displacement curve has a different shape in the initial and final phases. We do not think that the loss of elastic recoil energy is important in the in-plane tear test.

In summary, we find it plausible that differences between the critical fracture energy and total fracture energy arise from microscopic mechanisms. For example, when the entire fiber length is pulled out from the fracture line in the tear test, more energy may dissipate than in the measurement of critical fracture energy. This test measures the critical fracture energy at the onset of crack propagation when fibers across the crack tip may still be partially bonded. Microscopic roughness of the fracture line is another factor that may affect the tearing work more than the critical fracture energy. **TJ**

*Heikki Kettunen is acting as a research scientist at the Laboratory of Paper Technology, Helsinki University of Technology, Finland, and at KCL Paper Science Center, Box 70, FIN-02151 Espoo, Finland. Niskanen is a senior research scientist at KCL Paper Science Centre, Finland.*

*We thank Julien Doussot, who performed a large portion of the experimental work. Our study has received financial support from the Technology Development Center of Finland.*

*Received for review Sept. 18, 1998.*
*Accepted Nov. 16, 1998.*

### LITERATURE CITED

1. Kärenlampi, P., Suur-Hamari, H. T., Alava, M. J., *et al.*, *TAPPI J.* 79(5): 203(1996).
2. Unger, E., *Zellstoff und Papier* 9(3): 99(1960).
3. Van den Akker, J. A., Wink, W. A., and Van Eperen, R. H., *Tappi* 50(9): 446(1967).
4. Lyne, M. B., Jackson, M., and Ranger, A. E., *Tappi* 55(6): 924(1972).
5. Seth, R. S. and Page, D. H., *Tappi* 58(9): 112(1975).
6. Helle, T., *International Paper Physics Conference Proceedings*, CPPA, Montreal, 1979, 13.
7. Y.-W. Mai, *Appita* 36(6): 461(1983).
8. Kettunen, H. and Niskanen, K., "Fiber debonding along a crack front," in "Progress in Paper Physics Seminar" (abstracts only), TAPPI PRESS, Atlanta, 1998, B4.
9. Kärenlampi, P., Ph.D. thesis, Helsinki University of Technology, Laboratory of Paper Technology, 1996, p. 47.
10. Korteoja, M. J., Lukkarinen, A., Kaski, K., *et al.*, *TAPPI J.* 79(4): 218(1996).
11. Korteoja, M. J., Niskanen, K. J., Kortschot, M. T., *et al.*, *Paper and Timber* 80(5): 364(1997).
12. Seth, R. S., Robertson, A. G., Mai, Y.-W., *et al.*, *Tappi J.* 76(2): 109(1993).
13. Kärenlampi, P., Cichoracki, T., Alava, M., *et al.*, *TAPPI J.* 81(3): 155(1998).

## APPENDIX: MECHANICAL ANALYSIS OF TEAR TEST

We analyzed the quasistatic, uniaxial, and in-plane strain distribution in the in-plane tear test using the coordinate system defined in **Fig. A1**. The initial span length is $2H$, and the ligament length is $L$. The lateral coordinate $x$ measures the distance from the initial crack tip location. The mean strain $\varepsilon(x)$ corresponding to a given displacement of the two jaws, $2\,\Delta H$, is

$$\varepsilon(x) = \frac{\Delta H - x\tan\alpha}{H + x\tan\alpha} \qquad \text{(A1a)}$$

for $x \tan\alpha < \Delta H$ and

$$\varepsilon(x) = 0 \qquad \text{(A1b)}$$

otherwise.

We assume here that the specimen can buckle out of the plane, thereby relieving any compressive strain $\varepsilon < 0$. Equation A1 gives the mean strain value for a given $x$ because of the implicit assumption that $\varepsilon(x)$ is independent of $H$.

Assuming that the stress–strain relationship is linear, the external load $F$ is equal to the integral of local strain multiplied by the elastic modulus $E$ (Young's modulus by stretching):

$$F = \int_0^L E\,\varepsilon(x)\,dx \qquad \text{(A2)}$$

In the beginning, in the first phase of the test, the maximum value of $\varepsilon(x)$ is less than the critical strain $\varepsilon_c$ of fracture. In that case $F = F_1$ is given by

$$F_1 = \frac{E}{\tan\alpha}\left[(H+\Delta H)\,\ln\left(1+\frac{\Delta H}{H}\right) - \Delta H\right] \qquad \text{(A3)}$$

This equation applies when $\Delta H \le \varepsilon_c H$ and $\Delta H \le L \tan\alpha$. The latter condition ensures that the far end $x = L$ of the specimen is not strained. Equation A3 gives an essentially parabolic force–displacement curve, shown in **Fig. A2**. It differs from the linear trend assumed by Kärenlampi and coauthors (*1*).

The second phase in the force– displacement curve begins when the breaking limit $\varepsilon_c$ is exceeded and the crack begins to propagate. As long as the far edge of the specimen is slack, $\varepsilon_c H \le \Delta H \le L \tan\alpha$, we obtain $F = F_2$:

$$F_2 = \frac{E(H+\Delta H)}{\tan\alpha}\left[\ln(1+\varepsilon_c) - \frac{\varepsilon_c}{1+\varepsilon_c}\right] \qquad \text{(A4)}$$

In this phase, force increases slightly with the displacement. This increase occurs because the lateral length of the strained "neck" has increased.

Finally, the far edge of the specimen begins to tighten when $\Delta H > L \tan\alpha$. Force $F = F_3$ in the third phase is

$$F_3 = \frac{E}{\tan\alpha}\left\{(H+\Delta H)\ln\left[\frac{(L\tan\alpha + H)(1+\varepsilon_c)}{H+\Delta H}\right] + \frac{\Delta H - \varepsilon_c(H + L\tan\alpha) - L\tan\alpha}{1+\varepsilon_c}\right\} \qquad \text{(A5)}$$

This relationship corresponds again to parabolic behavior, though upside down compared to $F_1$.

The area under the force–displacement curve gives the total tearing work $W_{total}$. A straightforward calculation shows that

$$W_{total} = F_2 \cdot \Delta H_{total} = 2F_2 \cdot L\tan\alpha \qquad \text{(A6)}$$

According to Eq. A4, $F_2$ is inversely proportional to $\tan\alpha$. Thus, $W_{total}$ should be independent of the tearing angle $\alpha$. Thus, $2F_2 \cdot \tan\alpha$ should be equal to tearing work per unit crack length. Another way to estimate tearing work is to

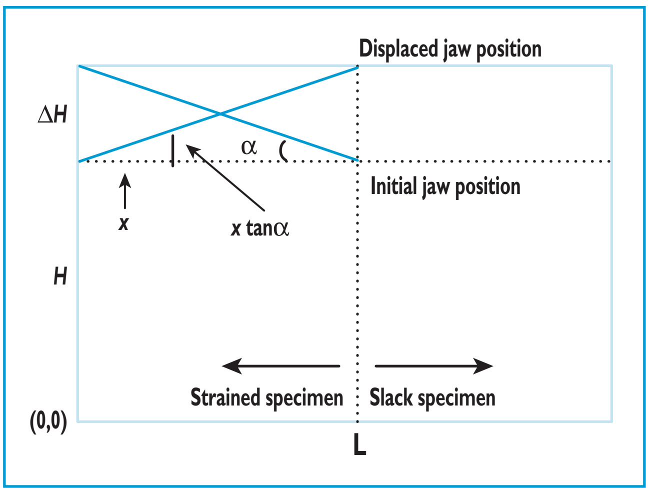


***A1. Coordinate system for calculating the stress distribution in the top half of a tear specimen. In the test, the top edge moves up. Origin x = H = 0 is at the initial crack tip. The part of specimen to the left of the tip is not shown.***

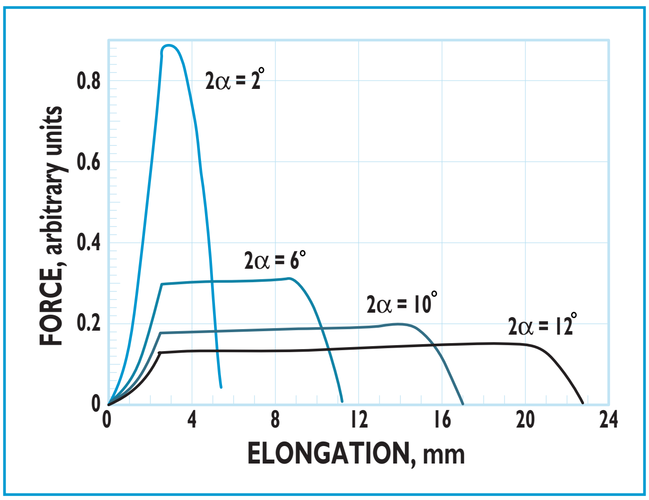


***A2. Tearing force vs. displacement of the jaws for a few tearing angles according to Eqs. A3–A5.***

use measurements at different $\alpha$ and determine the slope of $F_2$ against $\tan^{-1}\alpha$ by linear regression. We compare the two values in the experiments.

Equation A6 was derived under the assumption that the paper behaves linearly in regard to elastic stress–strain. However, one can easily see that nonlinearity would change only the first and third phases of the force–displacement curves in Fig. A2 from parabolic to S-shaped. The second phase would be almost unaffected, and therefore Eq. A6 should still be valid.

Nonlinear stress concentration at the crack tip would also alter the derivation. In reality, the local stress increases rapidly towards the crack tip. This increase can have two important effects. First, in principle, it can invalidate Eq. A6. However, we can reject this possibility as follows. First, we rewrite Eq. A2 using an effective span length $H_{eff}(x)$ instead of $H$, where $H_{eff}$ is implicitly defined by

$$F = E \int \frac{\Delta H - x\tan\alpha}{H_{\mathrm{eff}}}\, dx \qquad \text{(A7)}$$

We can then adjust $H_{eff}(x)$ so that we obtain the correct stress field along the mid-plane of the specimen. The result tearing force $F_2$ in Phase 2 will still be inversely proportional to $\tan\alpha$.

The second consequence of the stress concentration is the localization of the fracture process in a zone that is smaller than fiber length. In that case, the fracture process zone is microscopic and is not controlled by the stresses in the macroscopic continuum. Since the size of the fracture process zone decreases with increasing tearing angle, there must be a minimum value $\alpha_c$ such that the continuum picture is invalid for $\alpha \geq \alpha_c$. To estimate the threshold value of $\alpha$, we use a simple model for the stress concentration at the crack tip:

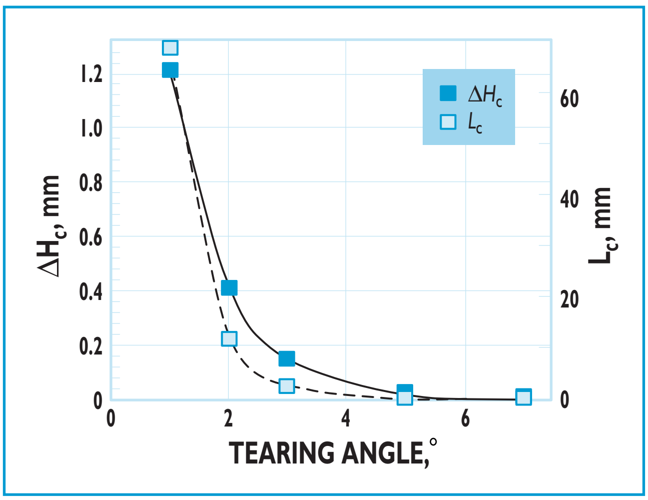


***A3. The critical displacement $\Delta H_c$ and the size of the fracture zone $L_c$ decrease with increasing tearing angle $\alpha$.***

$$\varepsilon(x,h) = A \cdot \frac{H+\Delta H}{(L-L_c)h + L_c(H+\Delta H)} \cdot \frac{\Delta H - x\tan\alpha}{H + x\tan\alpha} \qquad \text{(A8)}$$

where $L_c$ is the lateral length of the strained "neck" and $h$ is the longitudinal coordinate from the crack tip. In other words, $L_c$ is a measure of the size of the fracture process zone. We calculate the normalization constant $A$ by integrating the strain in the longitudinal direction according to Eq. A9:

$$\int_0^{H+\Delta H} \varepsilon(x,h)\, dh = \Delta H - x\tan\alpha \qquad \text{(A9)}$$

Integrating $x$ gives

$$\varepsilon(x,h) = (\Delta H - x\tan\alpha) \cdot \frac{(L-L_c)}{(L-L_c)h + L_c(H+\Delta H)} \cdot \left(\ln\frac{L}{L_c}\right)^{-1} \qquad \text{(A10)}$$

At the onset of crack propagation, $\varepsilon(0,0) = \varepsilon_c$. The corresponding displacement $\Delta H_c$ follows by solving Eq. A11 iteratively:

$$L\tan\alpha - \Delta H = \varepsilon\,(H+\Delta H)\,\ln\frac{L\tan\alpha}{\Delta H} \qquad \text{(A11)}$$

**Figure A3** illustrates how the calculated critical displacement $\Delta H_c$ and fracture zone size $L_c$ decrease with increasing $\alpha$. In the case shown, the fracture process zone becomes microscopically small already at $2\ \alpha_c \approx 2°$. (The ligament length was 80 mm, the span length was 40 mm, and the critical strain $\varepsilon_c$ was 3%.)

In summary, we find that the macroscopic continuum model is relevant only for very small tearing angles. In all other cases, microscopic network mechanics govern the fracture process. If out-of-plane deformations and energy dissipation outside the actual fracture process zone can be ignored, then the in-plane tear energy per unit crack length should be independent of the macroscopic test geometry. The true crack length, determined at the microscopic scale, may be larger than the ligament length of the macroscopic specimen. This condition will affect the work measured in a macroscopic tear test.